Monopod robot prototype with reaction wheel for hopping and posture stabilisation

Asahi Anzai*, Toshihide Doi and Kazuki Hashida

Graduate School of Science and Engineering,
Meiji University,
1-1-1 Higashi-Mita, Tama-ku,
Kawasaki-shi, Kanagawa, Japan
Email: ce202007@meiji.ac.jp
Email: wings104toshi@gmail.com
Email: light.shs.1103@gmail.com
*Corresponding author

Xuechao Chen and Lianqiang Han

School of Mechatronical Engineering,
Beijing Institute of Technology,
Beijing, 100081, China
Email: chenxuechao@bit.edu.cn
Email: hanlianqiang@bit.edu.cn

Kenji Hashimoto

Department of Mechanical Engineering Informatics,
Meiji University,
1-1-1 Higashi-Mita, Tama-ku,
Kawasaki-shi, Kanagawa, Japan
Email: hashimoto@meiji.ac.jp

Abstract: The purpose of this study is to develop a one-legged hopping robot, which has the fewest number of legs as a legged robot, and to realise hopping motion, upright posture stabilisation and getting up. The long-term goal is to develop biped robots and multi-legged robots capable of jumping and running. We designed and fabricated an electrically driven 2-DoF monopod MH-1 with pitch axes at the hip and knee joints equipped with a reaction wheel. MH-1 realised hopping while the robot is constrained so that it could only move in the vertical direction. We also proposed a control method for upright posture stabilisation and getting up of a monopod robot using a reaction wheel. MH-1 realised getting up and stabilising its upright posture within the range of the motor characteristics.

Keywords: monopod robot; hopping; reaction wheel; linear quadratic regulator; LQR; posture stabilisation.

Reference to this paper should be made as follows: Anzai, A., Doi, T., Hashida, K., Chen, X., Han, L. and Hashimoto, K. (2021) 'Monopod robot prototype with reaction wheel for hopping and posture stabilisation', *Int. J. Mechatronics and Automation*, Vol. 8, No. 4, pp.163–174.

Biographical notes: Asahi Anzai received her BE from the Department of Mechanical Engineering Informatics, Meiji University, Japan, in 2020. Currently, she belongs to the Department of Mechanical Engineering, The Graduate School of Science and Engineering, Meiji University as an ME student. Her research areas include legged robots, hopping and posture stabilisation.

Toshihide Doi received his ME from the Department of Mechanical Engineering, The Graduate School of Science and Engineering, Meiji University, Japan, in 2021. His research areas include legged robots and hopping.

Kazuki Hashida received his ME from the Department of Mechanical Engineering, The Graduate School of Science and Engineering, Meiji University, Japan, in 2020. His research areas include legged robots and posture stabilisation.

Xuechao Chen received his BS and PhD from the Beijing Institute of Technology (BIT), Beijing, China, in 2007 and 2013, respectively, both in Mechatronics Engineering. He was a visiting student with the Robotics Institute, Carnegie Mellon University, Pittsburgh, PA, USA, in 2012 and Visiting Scientist at Sibley School of Mechanical and Aerospace Engineering, Cornell University, Ithaca, USA, in 2018. He is currently an Associate Professor with the School of Mechatronical Engineering, BIT. His research interest includes biped locomotion.

Lianqiang Han received his BS in Mechatronics Engineering from the Beijing Institute of Technology (BIT), Beijing, China, in 2018. He is currently working towards a PhD in Biped Robot in the Intelligent Robotics Institute, with the School of Mechatronical Engineering, BIT. His research interests include motion planning, balance control, and dynamic working for a biped robot with joint torque control.

Kenji Hashimoto received his BE and ME in Mechanical Engineering, in 2004 and 2006, respectively, and PhD in Integrative Bioscience and Biomedical Engineering, in 2009, all from the Waseda University, Japan. He was an Assistant Professor from 2015 to 2017, and Associate Professor from 2017 to 2018 at the Waseda Institute for Advanced Study, Waseda University. In the April of 2018, he joined the Faculty of the Department of Mechanical Engineering Informatics, Meiji University, where he is currently an Associate Professor. His research interests include legged robots and humanoid robots.

This paper is a revised and expanded version of a paper entitled ‘Development of prototype electric-driven 2-DoF monopod robot for hopping motion’ presented at 2021 IEEE International Conference on Mechatronics and Automation (ICMA 2021), Takamatsu, Japan, 8–11 August 2021.

1 Introduction

Recently, there have been a lot of studies on mobile robots, which can be broadly divided into wheeled, crawler, flying, and legged. Wheeled robots can move fast on flat ground, but since wheeled robots always move in contact with the ground, it is difficult for them to move on rough terrain or climb up and down steps. Crawler robots are more adaptable to rough terrain than wheeled robots, but they are not good at descending steps and climbing up and down the spiral staircase. Flying robots can fly over rough terrain or steps, but it is difficult for them to perform manipulation work that requires a lot of power. On the other hand, legged robots can move on rough terrain that is difficult for wheeled robots. Legged robots can also climb up and down steps that is difficult for wheeled and crawler robots. This is because legged robots can choose discrete touchdown points by lifting their feet off the ground and grounding their feet again (Hardarson, 1997). Since legged robots are on the ground, they could potentially perform powerful manipulation tasks that are difficult for flying robots (Hashimoto et al., 2017).

Moreover, legged robots can perform dynamic locomotion such as jumping, running, and parkour because they can move flexibly with their legs. Legged robots that perform dynamic locomotion include Atlas of Boston Dynamics (2021), which can perform parkour, Cheetah of MIT (Seok et al., 2013; Park et al., 2017; Bledt et al., 2018), which can jump and move at high speed, ANYmal of ETH (Hutter et al., 2016), which has high mobility capabilities such as climbing up and down stairs and getting over obstacles, and SpaceBok (Kolvenbach et al., 2019), which can jump powerfully under low gravity. By studying legged robots with such high mobility, legged robots will be able to not only climb up and down steps and move on rough terrain, but also improve the moving speed. As for the moving speed, which is one of the problems of legged robots (Machado and Silva, 2006), integrating a high jumping motion into the running motion will make it possible to increase the running speed and improve the performance of legged robots as mobile robots.

As described above, legged robots have the potential to exceed the abilities of humans and animals and are expected to be applied in various fields such as disaster response, delivery, factory inspection, and operation in space environments. Legged robots are considered to have higher versatility than other types of mobile robots. Therefore, the long-term goal is to develop biped robots and multi-legged robots with high locomotion capabilities such as jumping and running. The objective of this study is to design and fabricate a prototype of a monopod hopping robot called Meiji Hopper – no. 1 (MH-1), which has the fewest number of legs as a legged robot. The motivation for developing a monopod robot is to understand more about the system dynamics of legged robots and obtain quantitative data from evaluation experiments in order to utilise the data to the development of biped robots and multi-legged robots. Since the dynamics, leg coordination and gait control become more complex as the number of legs increases (Sayyad et al., 2007), we will first develop a monopod robot that has the smallest number of legs in legged robots and allows only hopping.

In addition, a point-grounded monopod robot has an unstable equilibrium point and cannot stand stably in an upright position. Moreover, most of the previous studies on monopod robots have not considered the recovery from a fall. Therefore, another objective of this research is to achieve ‘upright posture stabilisation’ and ‘getting up from

a fallen state'. To achieve these goals, MH-1 is equipped with a reaction wheel. The reaction wheel is a disk with a large inertia, and the posture of the robot can be controlled by rotating it and generating a reaction torque. An example of a reaction wheel is the Cubli, developed by Gajamohan et al. (2012). In the long term, the goal is to use the reaction wheel to improve postural stability when the monopod robot is applied to bipedal robots or multi-legged robots.

Examples of monopod robot developments include 3D One-Leg Hopper developed by Raibert (1986), which is a monopod jumping robot using hydraulic actuators to drive the hip joint and pneumatic actuators for the linear motion mechanism, a biologically-inspired hopping robot Kenken developed by Hyon and Mita (2002), Salto and Salto-1P developed by Haldane et al. (2016, 2017), which are small monopod jumping robots with electric actuators, and more recently, a parallel legged monopod robot which can control its hopping height developed by He et al. (2021). We will follow these studies to develop a monopod hopping robot.

This paper is organised in the following contents. Section 2 explains mechanical design of MH-1 including the basic specifications and motor and gearhead selection. Section 3 describes the control method for upright posture stabilisation and getting up using reaction wheel. Section 4 contains the experiments and results for hopping, upright posture stabilisation and getting up. Section 5 concludes the paper and future works for further research.

2 Mechanical design of MH-1

2.1 Basic specifications

The height of MH-1 is about 500 mm, which is easy to experiment with. The mass of the leg should be as small as possible because the leg needs to move at high speed to achieve hopping motion. Considering the application to bipedal and multi-legged robots, the leg mechanism is a simple serial link mechanism with two links that has a wide range of motion. The ground contact is a point contact, which simplifies the leg mechanism and eases control of the robot by setting the ground plane to one point. Pitch axes are placed at the hip joint and knee joint, resulting in two degrees of freedom. Figure 1 shows the layout of the degrees of freedom. Two electric motors are used as leg actuators. Gearheads, timing belts and pulleys are used to decelerate and transmit power. Gearheads are compact and can save space. Timing belts and pulleys can transmit a large amount of force without backlash. MH-1 is equipped with a reaction wheel for the study of posture stabilisation and getting up. By using a reaction wheel, the same mechanism can be used for both posture stabilisation and getting up, which will lead to weight reduction and simplification. The reaction wheel rotates in the pitch direction and is active.

In this study, we need to design a guide that allows for two types of constraints depending on the experiments. When we evaluate whether MH-1 can perform hopping motion, its upper body part is attached to the guide to restrain the movement in the front-back and left-right directions. This allows MH-1 to move only in the up-down direction. When conducting experiments using a reaction wheel, MH-1 is limited to move in the sagittal plane. The motion of MH-1 can be constrained to translational motion in the front-back and up-down directions and rotational motion around the pitch axis.

Figure 1 Layout of the degrees of freedom (see online version for colours)

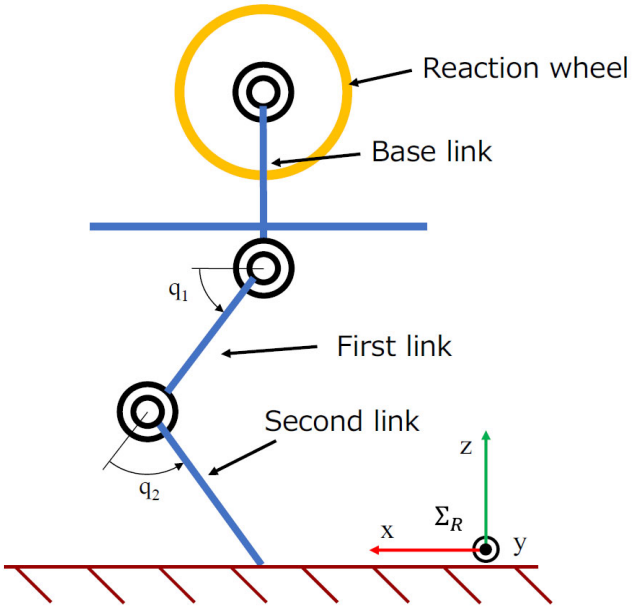

2.2 Meiji Hopper – no. 1 prototype (MH-1P)

In order to decide on the required specifications needed to select electric motors and gearheads for the hip and knee joints of MH-1, we have previously developed a monopod robot called Meiji Hopper – no. 1 prototype (MH-1P). MH-1P has two degrees of freedom by placing pitch axes at the hip joint and knee joint, using electric motors with sufficient power (EC-4pole 30, Maxon Motor Inc.). MH-1P is not equipped with a reaction wheel. Figure 2 shows the 3DCAD diagram of MH-1P. Timing belts and pulleys are used for deceleration. The rotational speed of the hip motor is reduced by three sets of belts and pulleys, with a reduction ratio of 3:1 in the first stage, 2:1 in the second stage, and 2.25:1 in the third stage, for a total deceleration of 13.5:1. The rotational speed of the knee motor is also reduced by three sets of belts and pulleys, with a reduction ratio of 3:1 in the first stage, 3:1 in the second stage, and 3:1 in the third stage, for a total of 27:1. The knee joint motor uses another set of a timing belt and pulleys with a reduction ratio of 1:1 to transmit power to the knee joint.

The total mass of MH-1P is 6.3 kg. The mass of the leg is 1.0 kg. The height from the ground to the top of the robot is 500 mm with the leg extended perpendicular to the ground. The length from the foot to the rotational axis of the knee joint and the length from the rotational axis of the knee joint to the rotational axis of the hip joint are both 150 mm. The upper body part of MH-1P is attached to restrain its

movement in the front-back and left-right directions. The hopping experiment was conducted with MH-1P moving only in the up-down direction. The plots in Figure 3 show the output torque and rotational speed obtained from the MH-1P hopping experiment. These data are used to select the motors and gearheads for MH-1 in Section 2.3.

Figure 2 3D CAD diagram of MH-1P (see online version for colours)

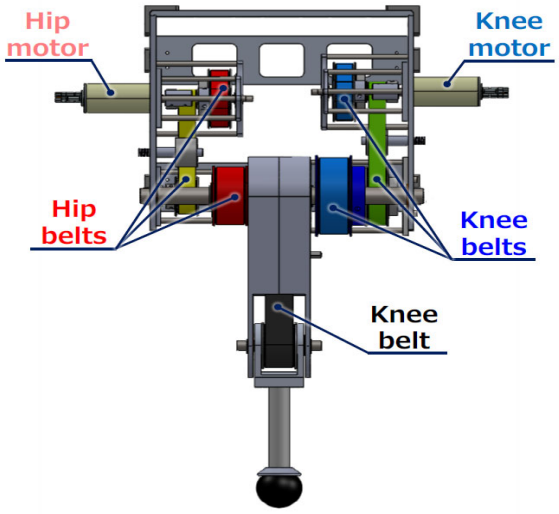

Figure 3 Speed-torque curve, (a) knee joint (b) hip joint (see online version for colours)

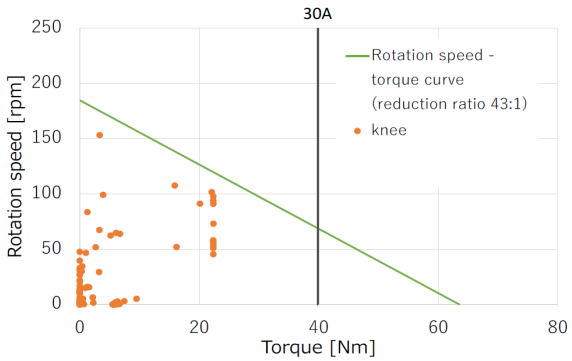

(a)

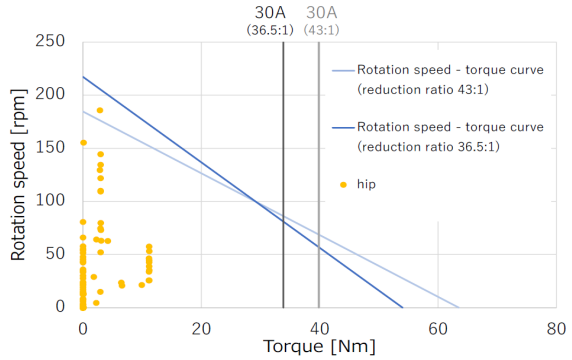

(b)

Note: The plots are the data obtained through the hopping experiment of MH-1P.

2.3 Motor and gearhead selection

The motors and gearheads for the knee and hip joints of MH-1 were selected based on the data of the rotational speed and torque output during hopping obtained from the hopping experiment of MH-1P. For both hip and knee joints of MH-1, DCX 35 L 80W/120W motors and GPX42 C 43:1 gearheads manufactured by Maxon Motor Inc. were selected. These are comparatively lightweight and powerful motors and gearheads. The specifications of the motors and gearheads selected for the hip and knee joints of MH-1 are shown in Tables 1 and 2. Figure 3 shows comparisons of the rotation speed-torque curve of the motor with the gearhead after reduction and the output torque and rotational speed obtained in the hopping experiment of MH-1P. The motor controllers are EPOS4 Compact 50/8 CAN manufactured by Maxon Motor Inc. It should be noted that the maximum output current of the EPOS4 Compact 50/8 CAN is 30 A. Therefore, the motor controllers cannot output torque that requires more current than 30 A. For the knee joint, the output torque and rotational speed of MH-1P were satisfied by the rotation speed-torque curve with 43:1 reduction by the gearhead. For the hip joint, the reduction ratio needed to be 36.5:1. The gearhead reduces the rotational speed to 43:1 and the timing belt and pulleys increase the rotational speed to 34:40 in order to satisfy the rotation speed-torque curve.

The motor and gearhead for the reaction wheel of MH-1 were selected based on the data of the rotation speed and torque output from the simulation of getting up. For the reaction wheel of MH-1, DCX 35 L 80W/120W motor and GPX42 C 4.3:1 gearhead manufactured by Maxon Motor Inc. were selected. Tables 1 and 3 show the specifications of the motor and gearhead of the reaction wheel.

Table 1 Motor specifications of MH-1

Model number	DCX 35 L 80W/120W
Nominal voltage (V)	36
Rated output (W)	80
Stall torque (mNm)	2,160
No load rotation speed (rpm)	7,940
Torque constant (mNm/A)	42.9
Weight (g)	385

Table 2 Gearhead specifications of MH-1 knee and hip joints

Model number	GPX42 C 43:1
Number of stages	3
Reduction ratio	43:1
Maximum intermittent torque (Nm)	22.5
Maximum intermittent input speed (rpm)	10,000
Maximum radial load (N)	360
Weight (g)	460

Table 3 Gearhead specifications of MH-1 reaction wheel

Model number	GPX42 C 4.3:1
Number of stages	3
Reduction ratio	4.3:1
Maximum intermittent torque (Nm)	4.5
Maximum intermittent input speed (rpm)	10,000
Maximum radial load (N)	120
Weight (g)	260

2.4 Mechanical design details of MH-1

Figure 4 shows the schematic diagram of the drive mechanism. As described in Section 2.3, MH-1 uses motors with gearheads having a reduction ratio of 43:1 for the hip and knee joints. The motor for the hip joint is placed above the motor for the knee joint. The timing belt and pulleys reduce the rotation speed of the hip motor to 34:40 and transmit it to the hip joint. The rotation shaft of the lower hip pulley is connected to the upper leg. The bearings prevent the shaft of the knee motor from interlocking with the rotation of the lower hip pulley. The motor for the knee joint is positioned so that the shaft of the knee motor is coaxial with the rotation shaft of the hip joint. The power of the knee motor is transmitted to the knee joint by means of a timing belt and pulleys with a reduction ratio of 1:1. The rotation shaft of the lower knee pulley is connected to the lower leg. The bearings prevent the rotation shaft of the lower knee pulley and the upper leg from rotating together.

Figure 4 Schematic diagram of drive mechanism of MH-1 (see online version for colours)

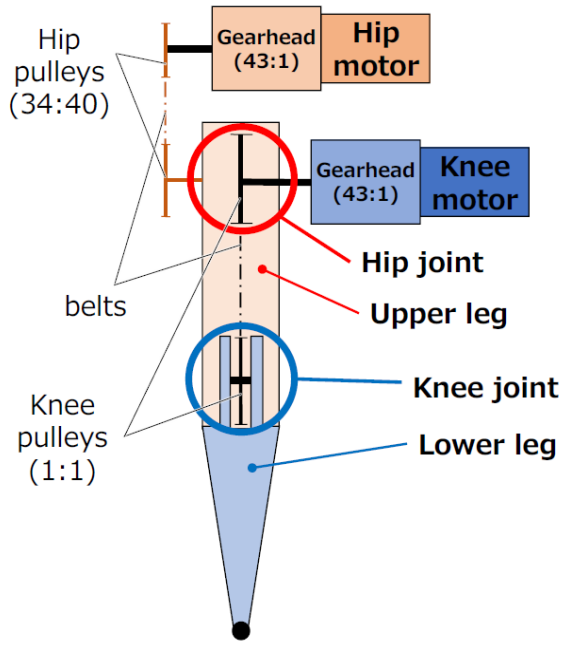

The 3D CAD diagram of MH-1 is shown in Figure 5. The timing belts used are Power Grip EV belt EV5GT type of Gates Unitta Asia Co., Ltd., which can save space with its small belt width and transmit a large amount of torque. For the timing pulleys, 5GT pulley is used, corresponding to EV5GT belt.

Figure 5 3D CAD diagram of MH-1 (see online version for colours)

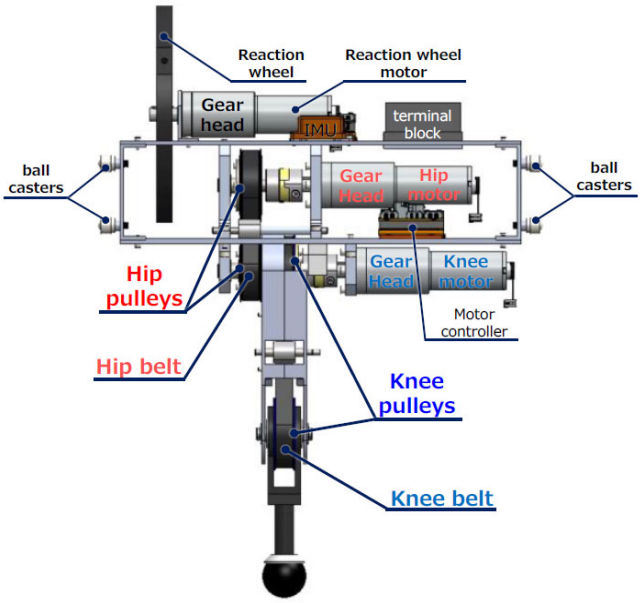

The upper leg parts, the upper part of the lower leg, and the upper body parts were made by cutting extra super duralumin, which is a lightweight and high strength aluminium alloy. As shown in Figure 5, three motors are attached to the upper body parts using motor mounts, two for the knee and hip joints and one for the reaction wheel for the study of posture stabilisation and getting up. Bearing holders are mounted on the opposite side of the motor mounts for the knee and hip motors to support the end of the motor shafts and avoid cantilever. The motor shafts are extended with the couplings because the length of the motor shafts themselves are short. The upper leg has a structure to pass a timing belt inside. Two tensioners are placed between the two pulleys for the knee joint to apply tension to the knee belt. Another tensioner is installed between the two pulleys for the hip joint, which also provides tension to the hip belt. A carbon fibre reinforced plastics (CFRP) pipe is used for the lower leg to reduce weight. The CFRP pipe is glued to the foot part and the upper part of the lower leg, which is connected to the lower knee pulley. Figure 6 shows foot parts and a cross-sectional view of a plastic insert. A squash ball and a plastic insert are used for the foot part, referring to the Mini Cheetah of MIT (Katz, 2018). The plastic insert was formed by a 3D printer because it has a complicated shape with several holes to be filled with urethane foam. The plastic insert was inserted into the squash ball with a drilled hole. The gap between the squash ball and the plastic insert was filled with urethane foam Smooth-On FlexFoam-It 23.

Figure 6 Foot part of MH-1, (a) plastic insert and foot part (b) cross-sectional view of plastic insert (see online version for colours)

(a)

(b)

As for the reaction wheel, one of the required specifications is to have as large a moment of inertia as possible. The larger the moment of inertia, the smaller the required motor output, and the requirement for the motor rotation speed and torque can be eased. To avoid interfering with the movement of the knee and hip joints and to make the leg lighter, the reaction wheel is placed on the upper part of the MH-1. The diameter of the reaction wheel was determined to be 200 mm so that the size of MH-1 including the reaction wheel would be around 500 mm. The wheel had to be designed to be heavier at the circumference and lighter at the centre in order to increase the moment arm. The wheel is divided into three parts: the boss, which is connected to the output shaft of the motor, the rim, which is the outer circumference of the wheel, and the spokes, which connect the boss and rim. The mass of each part was adjusted by using different materials. The boss and spokes are made of aluminium to reduce mass. The rim is made of brass to increase mass.

2.5 Meiji Hopper – no. 1 (MH-1)

Figure 7 shows the assembled MH-1. MH-1 is equipped with a reaction wheel for the study of stabilisation of a monopod robot. The height of MH-1 including the reaction wheel is 510 mm. The total mass of MH-1 including the reaction wheel is 6.9 kg. The mass excluding the reaction wheel and the motor and gearhead for the reaction wheel is 5.5 kg. The mass of the leg of the movable part is 0.9 kg. The length from the foot to the rotational axis of the knee joint and the length from the rotational axis of the knee joint to the rotational axis of the hip joint are both 150 mm. The diameter of the reaction wheel is 200 mm, and its mass is 0.7 kg.

Figure 7 Assembled MH-1 (see online version for colours)

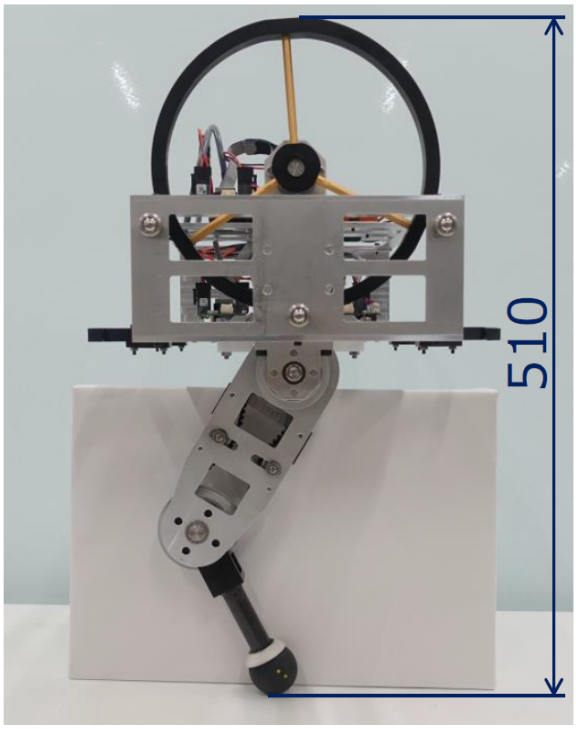

As described in Section 2.1, MH-1 requires the following two types of constraints:

1 Constrain the motion in the front-back and left-right directions so that it can move only in the up-down direction.

2 Constrain the motion to translational motion in the vertical and front-back directions and rotational motion around the pitch axis.

Figure 8 shows MH-1 attached to the linear guide. Figure 9 shows MH-1 placed in the guide consisting of two acrylic panels. The guide is assembled with aluminium frames and has both types of constraints. As for the first constraint, linear guides are attached vertically to the left and right sides of the right end of the guide. A linear guide is a mechanical component that moves smoothly without rattling in the direction of the rail. In this case, two linear guides are used so that the linear guide blocks can move precisely on the rails. MH-1 is attached to the blocks of the linear guide, which restrict the movement of MH-1 in the front-back and left-right directions and allow MH-1 to move smoothly only in the up-down direction. As for the second constraint, two acrylic panels are placed parallel to each other. MH-1 with ball casters is placed between two acrylic panels. The distance between the panels is set to be the depth of MH-1 including the ball caster so that translational

motion in the left-right direction and rotational motion around the roll and yaw axes are not possible.

Figure 8 MH-1 attached to the linear guide (see online version for colours)

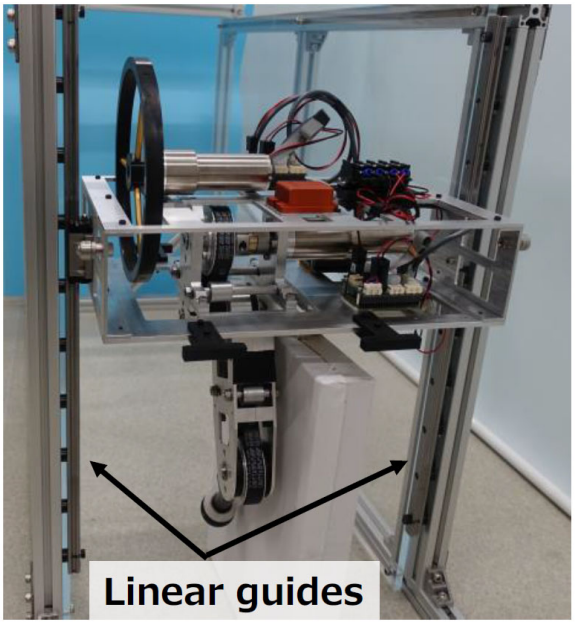

Figure 9 MH-1 placed in the guide consisting of two acrylic panels (see online version for colours)

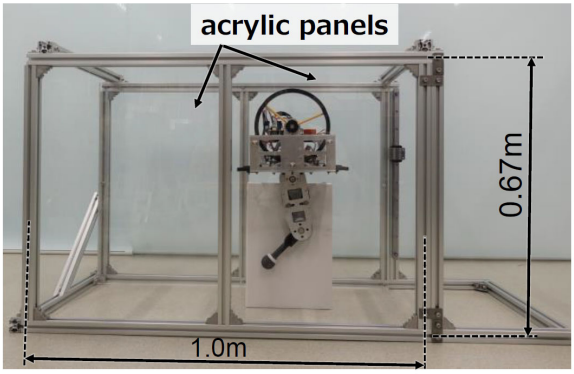

Figure 10 System configuration diagram (see online version for colours)

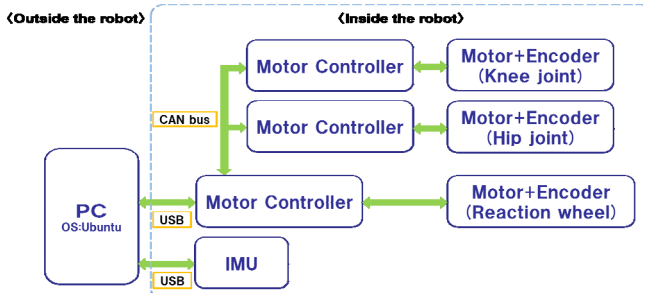

Figure 10 shows the system configuration diagram of MH-1. A PC controls three sets of motors and encoders via motor controllers. The first motor controller for the reaction wheel is connected to the PC via USB. The other two motor controllers for the hip and knee joints are connected to the first motor controller for the reaction wheel via CANopen. Angle and angular velocity information can be obtained from each encoder via the motor drivers. The IMU (Xsens, MTi30) for measuring the tilt of the body is connected to the PC via USB. The IMU is used in the experiment of upright stabilisation and getting up using a reaction wheel and is not used in the hopping experiment.

3 Control method using a reaction wheel

3.1 Monopod robot model

The main parameters of the monopod robot model are shown in Table 4. The parameters are based on the values of MH-1. Here, I_B and I_W represents the moment of inertia around the centre of gravity of the base link and reaction wheel. The other parameters are defined as shown in Figure 11. The monopod robot model consists of four parts: the base link, the first and second links which are the legs, and the reaction wheel attached to the base link. As described in Section 2.1, the model has three degrees of freedom around the pitch axes and are active. The ground contact is a point contact. The motion of the monopod robot model is limited to the sagittal plane. The ground surface should be sufficiently hard and uniformly flat.

3.2 Upright posture stabilisation

In this study, the monopod robot model is treated as an inverted pendulum to achieve upright posture stabilisation. Figure 12 shows a schematic diagram of the approximated robot model. Since the monopod robot model is point-grounded, the motion of the robot when it is upright can be regarded as an inverted pendulum with variable link length, as shown in Figure 12. Furthermore, we assume that all the mass of the robot, except for the reaction wheel, is concentrated at a one point, and the reaction wheel has a link with mass attached to its end point. The link shown in blue in Figure 12 is called ‘body’ and the link shown in green is called ‘wheel’.

Table 4 The main parameters of the monopod robot model

L_B (m)	0.12
L_{Bg} (m)	0.064
L_1 (m)	0.15
L_2 (m)	0.15
L_{1g} (m)	0.069
L_{2g} (m)	0.056
W_B (m)	0.34
m_B (kg)	5.4
m_1 (kg)	0.79
m_2 (kg)	0.13
m_W (kg)	0.7
I_B (kg·m^2)	0.023
I_W (kg·m^2)	0.0063

Figure 11 Parameters of the robot (see online version for colours)

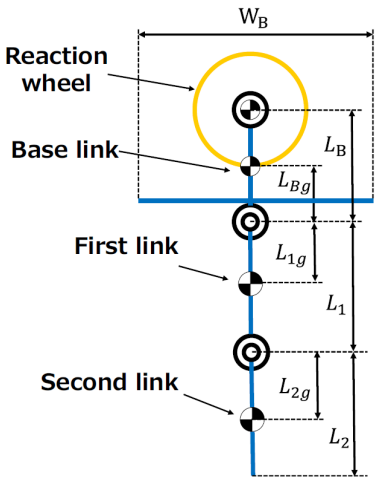

Figure 12 Approximate model of a monopod robot (see online version for colours)

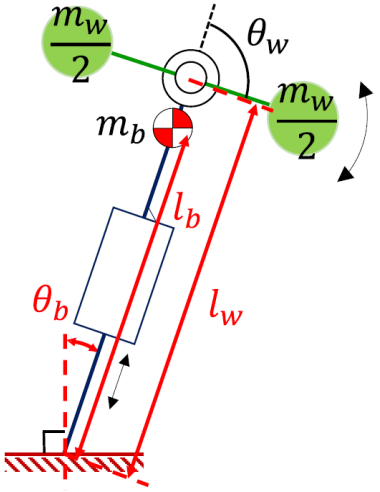

We derive the equation of motion from the Lagrange equation. First, let K_b be the kinetic energy of the body, K_w be the kinetic energy of the wheel. The kinetic energy of the system is as follows:

$$\begin{cases} K_b = \frac{1}{2} m_b \left(V_{bx}^2 + V_{by}^2 \right) + \frac{1}{2} \hat{I}_b \dot{\theta}_b^2 \\ K_w = \frac{1}{2} m_w \left(V_{wx}^2 + V_{wy}^2 \right) + \frac{1}{2} I_w \left(\dot{\theta}_b + \dot{\theta}_w \right)^2 \end{cases}, \tag{1}$$

where m_b is the mass of the body, m_w is the mass of the wheel, V_{bx} and V_{by} are the translational velocity of the centre of gravity of the body, V_{wx} and V_{wy} are the translational velocity of the centre of gravity of the wheel, $\hat{I}_b$ is the moment of inertia around the centre of gravity of the body, I_w is the moment of inertia around the rotation axis of the reaction wheel, θ_b is the angle formed by the straight line from the foot to the centre of gravity of the body and the vertical line, θ_w is the angle formed by the body and the wheel. Let l_w be the distance from the foot to the centre of rotation of the wheel and l_b be the distance from the foot to the centre of gravity of the body. Since $V_{bx}^2 + V_{by}^2 = l_b^2 \dot{\theta}_b^2$, $V_{wx}^2 + V_{wy}^2 = l_w^2 \dot{\theta}_b^2$, the equation (1) can be transformed as follows:

$$\begin{cases} K_b = \frac{1}{2} \left(m_b l_b^2 + \hat{I}_b \right) \dot{\theta}_b^2 = \frac{1}{2} I_b \dot{\theta}_b^2 \\ K_w = \frac{1}{2} \left(m_w l_w^2 + I_w \right) \dot{\theta}_b^2 + I_w \dot{\theta}_b \dot{\theta}_w + \frac{1}{2} I_w \dot{\theta}_w^2 \end{cases}, \tag{2}$$

where I_b is the moment of inertia of the body around the foot, and the centre of gravity of the wheel is assumed to be at the centre of rotation of the wheel. Second, the potential energy of the system U can be written as follows:

$$U = m_b l_b g \cos\theta_b + m_w l_w g \cos\theta_b = \left(m_b l_b = m_w l_w \right) g \cos\theta_b \tag{3}$$

From equations (2) and (3), the Lagrangian L of this system is as follows:

$$\begin{aligned} L = {} & \frac{1}{2} I_b \dot{\theta}_b^2 + \frac{1}{2} \left(m_w l_w^2 + I_w \right) \dot{\theta}_b^2 + I_w \dot{\theta}_b \dot{\theta}_w \\ & + \frac{1}{2} I_w \dot{\theta}_w^2 - \left(m_b l_b + m_w l_w \right) g \cos\theta_b \end{aligned} \tag{4}$$

The Lagrange equation is as follows:

$$\frac{d}{dt} \left(\frac{\partial L}{\partial \dot{\Theta}_i} \right) - \frac{\partial L}{\partial \Theta_i} = Q_i, \tag{5}$$

where $\Theta_i = [\theta_b \ \theta_w]^T$, $Q_i = [0 \ \tau_m]^T$, and τ_m is the input torque of the wheel. From the equations (4) and (5), the equation of motion for this monopod robot model can be derived as follows:

$$\begin{cases} \left(m_w l_w^2 + I_w + I_b \right) \ddot{\theta}_b + I_w \ddot{\theta}_w \\ -\left(m_b l_b + m_w l_w \right) g \sin\theta_b = 0 \\ I_w \ddot{\theta}_b + I_w \ddot{\theta}_w = \tau_m \end{cases} \tag{6}$$

Here, we use a linear quadratic regulator (LQR) as a stabilisation method. LQR is an infinite time optimal control, which enables to find a feedback gain K that stabilises the controlled system. The feedback gain K can be obtained by finding the optimal input $u = -Kx$ that minimises the following evaluation function.

$$J = \int_0^\infty \left\{ x^T Q x + u^T R u \right\} dt \tag{7}$$

where Q and R are weight matrices. The reason for adopting this method is that it can theoretically guarantee stability without the need for complicated work such as gain adjustment in PID control or pole assignment in state feedback control. To use LQR, the system matrix A and the control matrix B of the system need to be obtained. Therefore, equation (6) is solved for $\ddot{\theta}_b$ and $\ddot{\theta}_w$ and linearised to form a state space model as follows:

$$\dot{\mathbf{x}}(t) = \mathbf{A}\mathbf{x}(t) + \mathbf{B}u(t), \tag{8}$$

where

$$\mathbf{x} = \begin{bmatrix} \theta_b \\ \dot{\theta}_b \\ \dot{\theta}_w \end{bmatrix},$$

$$\mathbf{A} = \begin{bmatrix} 0 & 0 & 0 \\ \dfrac{(m_b l_b + m_w l_w) g}{I_b + m_w l_w^2} & 0 & 0 \\ \dfrac{(m_b l_b + m_w l_w) g}{I_b + m_w l_w^2} & 0 & 0 \end{bmatrix},$$

$$\mathbf{B} = \begin{bmatrix} 0 \\ -\dfrac{1}{I_b + m_w l_w^2} \\ \dfrac{I_b + I_w + m_w l_w^2}{I_w (I_b + m_w l_w^2)} \end{bmatrix}.$$

3.3 Getting up

As in the stabilisation of upright posture, if sufficient reaction force can be obtained by the reaction wheel, the necessary energy can be obtained even when recovering from a fall. However, a large amount of torque and rotation speed is required to get up MH-1, which may require values that exceed the output characteristics of the motor. To solve this problem, there have been several reports on the realisation of getting up by suddenly stopping a reaction wheel rotating at high speed (Gajamohan et al., 2012; Mitani et al., 2016). In these cases, a brake mechanism to stop the reaction wheel is separately prepared to generate the large angular momentum necessary for getting up. We considered using a similar mechanism, but the mass of MH-1 is larger than that of the machines in the previous studies, which increases the angular momentum required to get up. The specifications required for the brake part, such as torque and shock resistance, become more stringent. In addition, there is a problem that the mass of the robot would increase when a brake mechanism is installed. Since we considered that it was difficult to realise getting up by using only a reaction wheel, we propose a method to realise getting up by using not only the wheel but also the leg.

Specifically, the proposed method uses the leg to shift the ground point and make l_b and θ_b smaller, and thereby reducing the torque required to get up. Figure 13 shows the motion plan for getting up. The hip joint is moved in the fallen state (posture *A*), and the foot is brought closer to the base link (posture *B*). In this way, the distance from the foot to the centre of gravity becomes shorter, and θ_b becomes smaller. After this, MH-1 gets up by applying torque to the wheel and hip joint (posture *C*) and then moves to the upright state (posture *D*). As l_b becomes smaller, the moment of inertia around the centre of rotation, which is the ground contact point of the foot, becomes smaller. The torque required for getting up becomes smaller. As θ_b becomes smaller, the difference in potential energy from the fallen state to the upright state becomes smaller. The torque required for getting up becomes smaller. Therefore, if the posture is changed appropriately, getting up can be achieved with less torque.

Figure 13 Motion plan for getting up (see online version for colours)

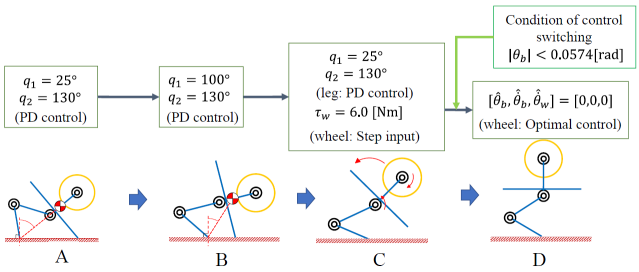

As shown in Figure 13, the angles of the knee and hip joints are tracked to their respective target angles by PD control. When the robot gets up (posture *C*), the torque is applied to the wheel by step input. When the body angle θ_b becomes small enough, the control is switched to optimal control to stabilise the posture. The range of the linear approximation is defined so that the approximation $\sin \theta_b \approx \theta_b$ with an accuracy of three significant digits, and the control is switched when $|\theta_b| < 0.0574$ [rad].

4 Experiments and results

4.1 Hopping

We tested whether MH-1 could realise hopping. Figure 14 shows the posture change of MH-1 during the experiment. The angles q_1 and q_2 shown in Figure 14 are changed from the initial angles q_1 = 50 deg and q_2 = 80 deg to the target angles q_1 = 80 deg and q_2 = 20 deg to make sure that the floor reaction force is applied directly below the hip joint. Figure 15 shows the flow of position control from the initial angle to the target angle, which is the position controller with feed-forward (Maxon Motor Inc., 2021). The acceleration and velocity feed-forwards and the PID controller output current. The position controller is implemented as a PID controller. The position control is interpolated by feed-forward control to improve the follow-up to the target values. The gain was determined by trial-and-error with $K_P = 20{,}000$, $K_i = 10{,}000$, $K_d = 100$.

The floor reaction force obtained from the force plate (CFP600XS302US made by Leptrino Inc.) is shown in Figure 16. The floor reaction force in the vertical direction at 0 s to 0.1 s and 0.5 s to 0.6 s is about 68 N, which is close to the value of 6.9 kg (mass of the robot) × 9.8 m/s^2 (gravity acceleration) = 67.62 N. The floor reaction force becomes small when the robot starts hopping, and it becomes 0 N at around 0.3 s. When the floor reaction force is 0 N, it means that the foot is off the ground. It can be judged that the hopping motion has been realised. In addition, Figure 17 shows a sequence of photographs of the hopping motion. The photographs also show that the foot is off the ground.

Figure 14 Posture change of the monopod robot (see online version for colours)

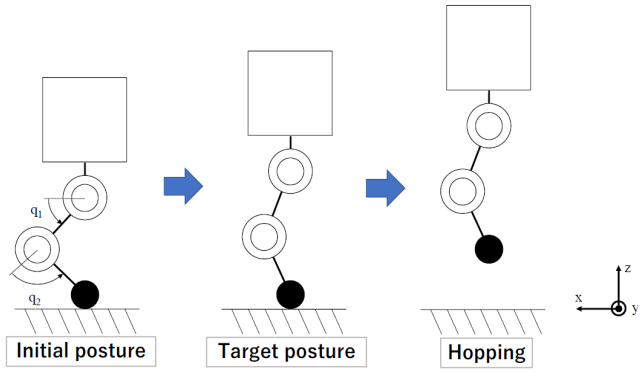

Figure 15 Position controller (see online version for colours)

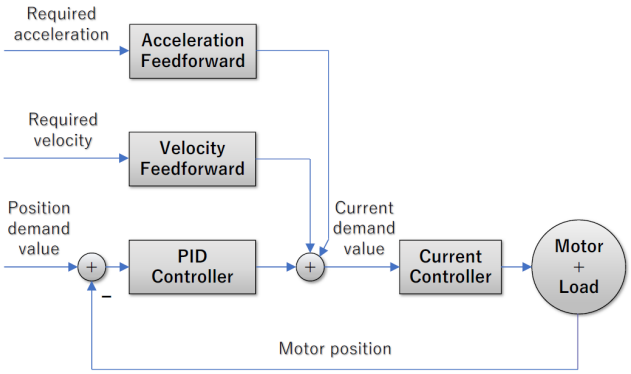

Source: Maxon Motor Inc. (2021)

Figure 16 Floor reaction force during hopping (see online version for colours)

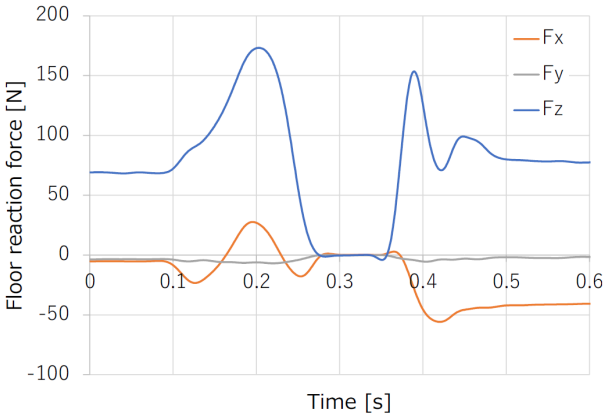

4.2 *Upright posture stabilisation*

We tested whether MH-1 could stabilise upright with its leg extended. Figure 18 shows the body angle θ_b the body angular velocity $\dot{\theta}_b$, the wheel angular velocity $\dot{\theta}_w$, the wheel input torque τ_w and the wheel command torque $\hat{\tau}_w$ obtained from the simulation and the experiment with MH-1, respectively. The body angle θ_b and the body angular velocity $\dot{\theta}_b$ are measured in the MH-1 experiment by the IMU mounted on the upper part of MH-1. From the graph, it can be seen that the body angle starts to converge in about three seconds, but the rotation speed of the wheel continues to increase and eventually it is no longer able to follow the command torque.

Figure 17 A sequence of photographs of the hopping motion (see online version for colours)

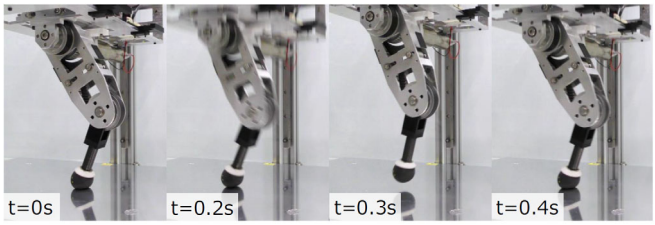

Figure 18 Results of upright posture stabilisation experiment, (a) body angle θ_b (b) body angular velocity $\dot{\theta}_b$ (c) reaction wheel rotation speed (d) command value $\hat{\tau}_w$ and measured value τ_w of torque to the reaction wheel (see online version for colours)

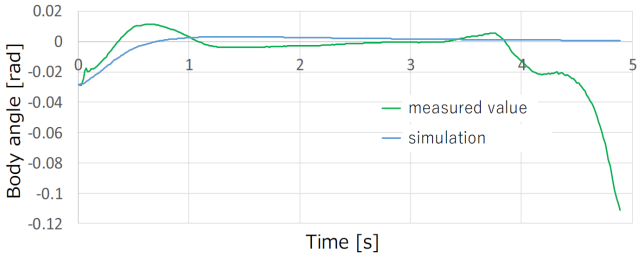

(a)

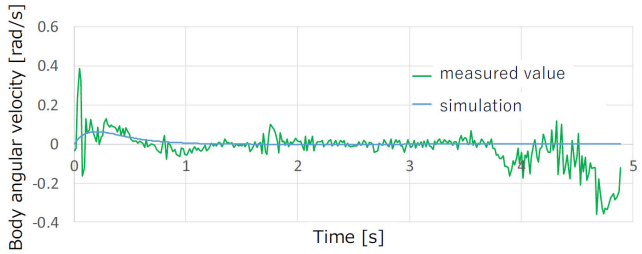

(b)

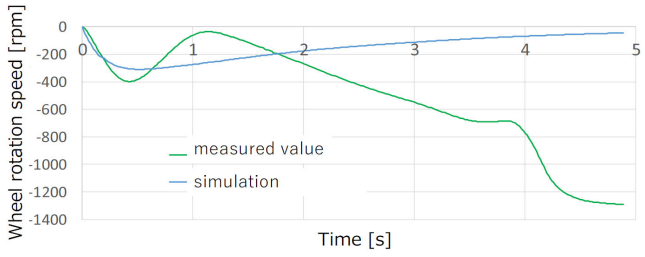

(c)

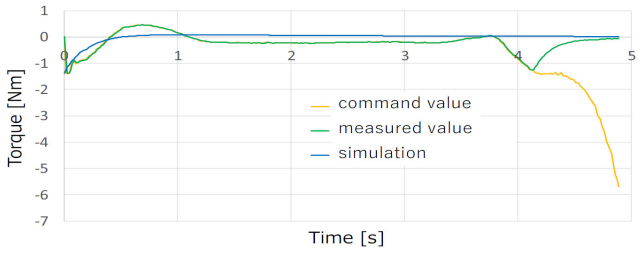

(d)

One possible cause is the limitation of the motor rotation speed-torque characteristics. Figure 19 shows the rotation speed-torque curve of the reaction wheel motor of MH-1. The horizontal axis is the torque [Nm] and the vertical axis is the rotation speed [rpm]. The red line represents the ideal characteristics based on the datasheet. The green plot is the actual measured values. From the graph, it can be seen that the limit of the rotation speed is reached at a value lower than the ideal straight line. This is thought to be caused by the inability to obtain sufficient rotation speed due to the back electromotive force of the motor.

Figure 19 Rotation speed-torque characteristics of wheel motor and measured values in upright posture stabilisation experiment (see online version for colours)

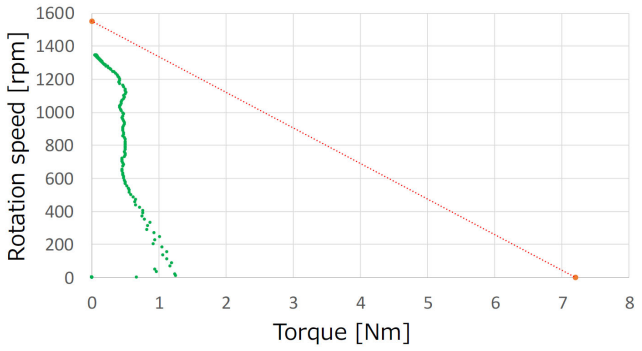

4.3 Getting up

We tested whether the MH-1 could get up. The purpose of this experiment is to verify whether the body angle can reach around the equilibrium point and exceed the threshold value. Even if θ_b exceeds the threshold value, the control is not switched to upright stabilisation control in this experiment.

Figure 20 shows a series of photographs of the getting-up motion. Figure 21 shows the measured body angle θ_b. As shown in Figure 20, the method proposed in Section 3.3 was able to achieve MH-1 getting up. The graph in Figure 21 shows that the body angle θ_b can be reduced by changing the posture using the leg. It can be confirmed that θ_b can be made to reach the threshold of the dashed line in the graph of Figure 21.

Figure 20 A series of photographs of the getting-up motion (see online version for colours)

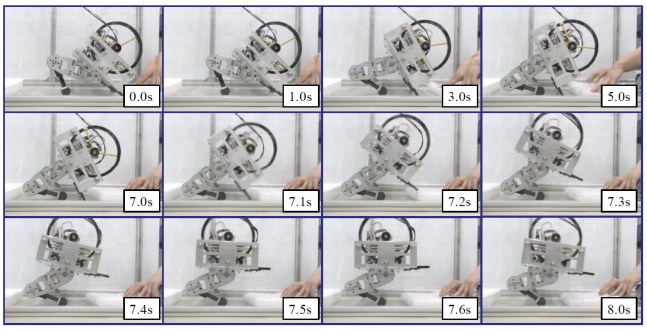

Figure 21 Result of getting up experiment (see online version for colours)

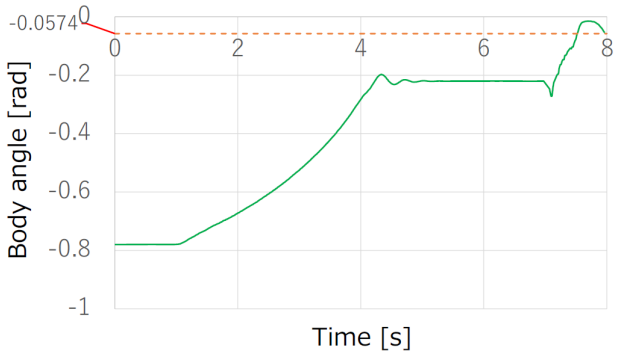

4.4 Discussion

From the above experiment, it is confirmed that MH-1 can hop while MH-1 is constrained so that it could only move in the vertical direction. This indicates that the mechanical design of MH-1 was minimally sufficient to perform the hopping motion. Although MH-1 has achieved hopping motion, the hopping height is still low. It is expected to increase the hopping height by improving the hardware, including re-selection of lighter and more powerful motors, and development of the hopping motion control. In addition, landing impact is large because landing control is not built in. It will be possible to predict landing and control the system to lessen the impact of landing by installing a distance sensor that detects the road surface.

MH-1 also realised getting up by using the leg and the reaction wheel. Changing the joint angles of the leg to reduce the moment of inertia made it possible to reduce the output of the motor for the reaction wheel required to get up. Furthermore, the reaction wheel allowed MH-1 to stabilise its upright posture within the characteristics of the motor for the reaction wheel. It is expected that the MH-1 can maintain an upright posture more stably and stabilise its posture after getting up from a fall by conducting a simulation that considers the back electromotive force of the motor and selecting an appropriate motor for a reaction wheel.

5 Conclusions and future work

We developed MH-1, a prototype of an electrically driven 2-DoF monopod robot with pitch axes at the hip and knee joints on the basis of the simulation and experimental results of the prototype called MH-1P. From the experimental results of MH-1, we confirmed that hopping was achieved by the actual robot. In addition, we proposed a method for stabilising the upright position and getting up using a reaction wheel. Getting up was achieved by simulation and the experiment of MH-1. As for upright posture stabilisation, it was confirmed that MH-1 can stabilise its upright posture within the range of the motor characteristics.

We are currently working on the development of Meiji Hopper – no. 2 (MH-2), a monopod robot equipped with a distance sensor that can predict landing and lessen landing

impact by detecting the road surface. In the future, we will consider changing the link mechanism and the number of degrees of freedom, adding elastic elements to the legs, and installing external sensors. In addition to the hardware improvement, we will develop the control system for online motion generation, improvement of hopping height and posture stabilisation, and realisation of continuous hopping.

Acknowledgements

This work was performed under the Research Cluster for Autonomous Robotic Systems, Meiji University. This work was supported by JSPS KAKENHI Grant Numbers JP20H04267, JP21H05055. This work was also supported by the National Key Research and Development Project under Grant 2018YFE0126200.

References

Atlas of Boston Dynamics (2021) [online] https://www.bostondynamics.com/atlas (accessed 31 August 2021).

Bledt, G. et al. (2018) 'MIT Cheetah 3: Design and control of a robust, dynamic quadruped robot', in *Proceedings of IEEE/RSJ International Conference on Intelligent Robots and Systems (IROS)*, pp.2245–2252.

Gajamohan, M. et al. (2012) 'The cubli: a cube that can jump up and balance', in *Proceedings of IEEE/RSJ International Conference on Intelligent Robots and Systems (IROS)*, pp.3722–3727.

Haldane, D.W. et al. (2016) 'Robotic vertical jumping agility via series-elastic power modulation', *Science Robotics*, Vol. 1, No. 1, pp.1–9.

Haldane, D.W., Yim, J.K. and Fearing, R.S. (2017) 'Repetitive extreme-acceleration (14-g) spatial jumping with Salto-1P', in *Proceedings of IEEE/RSJ International Conference on Intelligent Robots and Systems (IROS)*, pp.3345–3351.

Hardarson, F. (1997) *Locomotion for Difficult Terrain*, Technical Report, Mechatronics Division, Department of Machine Design, Royal Institute of Technology, Stockholm, Sweden.

Hashimoto, K. et al. (2017) 'WAREC-1 – a four-limbed robot having high locomotion ability with versatility in locomotion styles', in *Proceedings of IEEE International Symposium on Safety, Security and Rescue Robotics (SSRR)*, pp.172–178.

He, Z. et al. (2021) 'Controllable height hopping of a parallel legged robot', *Applied Sciences*, Vol. 11, No. 4, p.1421.

Hutter, M. et al. (2016) 'ANYmal – a highly mobile and dynamic quadrupedal robot', in *Proceedings of IEEE/RSJ International Conference on Intelligent Robots and Systems (IROS)*, pp.38–44.

Hyon, S.H. and Mita, T. (2002) 'Development of a biologically inspired hopping robot – 'Kenken'', in *Proceedings of IEEE International Conference on Robotics and Automation (ICRA)*, pp.3984–3991.

Katz, B.G. (2018) *A Low Cost Modular Actuator for Dynamic Robots*, Master's thesis, Massachusetts Institute of Technology.

Kolvenbach, H. et al. (2019) 'Towards jumping locomotion for quadruped robots on the moon', in *Proceedings of IEEE/RSJ International Conference on Intelligent Robots and Systems (IROS)*, pp.5459–5466.

Machado, J.A.T. and Silva, M.F. (2006) 'An overview of legged robots', in *Proceedings of the MME International Symposium on Mathematical Methods in Engineering*.

Maxon Motor Inc. (2021) *EPOS4 Positioning Controllers Application Notes* [online] https://www.maxongroup.es/medias/sys_master/8825356812318.pdf (accessed 31 August 2021).

Mitani, S. et al. (2016) 'High-agility, miniaturized attitude control sensors and actuators in an all-in-one module', *Transactions of the Japan Society for Aeronautical and Space Sciences, Aerospace Technology Japan*, Vol. 14, No. ISTS30, pp.47–53.

Park, H.W., Wensing, P.M. and Kim, S. (2017) 'High-speed bounding with the MIT Cheetah2: control design and experiments', *The International Journal of Robotics Research*, Vol. 36, No. 2, pp.167–192.

Raibert, M.H. (1986) *Legged Robots That Balance*, The MIT Press, Cambridge, MA.

Sayyad, A., Seth, B. and Seshu, P. (2007) 'Single-legged hopping robotics research – a review', *Robotica*, Vol. 25, No. 5, pp.587–613.

Seok, S. et al. (2013) 'Design principles for highly efficient quadrupeds and implementation on the MIT Cheetah robot', in *Proceedings of IEEE International Conference on Robotics and Automation (ICRA)*, pp.3307–3312.